# Spinodal Decomposition in a Subsurface Layer of a Polymer Blend Film

**Jakob Heier and Edward J. Kramer***

*Department of Materials, University of California at Santa Barbara, Santa Barbara, California 93106*

**Peter Revesz**

*Cornell Center for Materials Research, Cornell University, Ithaca, New York 14853*

**Gabor Battistig**

*MTA-Research Institute for Technical Physics and Materials Science, H-1525 Budapest, Hungary*

**Frank S. Bates**

*Department of Chemical Engineering and Materials Science, University of Minnesota, Minneapolis, Minnesota 55455*

*Received November 4, 1998; Revised Manuscript Received March 15, 1999*

ABSTRACT: We have studied phase separation in off-critical mixtures of poly(ethylene propylene) (hPEP) and perdeuterated poly(ethylene propylene) (dPEP) inside the metastable and unstable region of the phase diagram but under the influence of a surface that attracts the majority component (dPEP). In the adjacent depletion region nucleation barriers are eliminated, and the film starts to phase separate long before phase separation occurs in the bulk. The hPEP-rich domains are confined to grow anisotropically within the unstable region. The growth gives rise to the formation of a regular roughness pattern on the surface when the domains relax into a more circular shape driven by interfacial tension. The volume fraction versus depth profiles are obtained using time-of-flight forward recoil spectrometry (TOF-FRES) while the roughness pattern that mirrors the phase morphology in the depletion layer can be monitored by scanning force microscopy (SFM). Depending on initial dPEP volume fraction the lateral bicontinuous phase pattern inside the unstable region either develops into a dPEP-rich layer containing hPEP-rich droplets or forms a continuous hPEP-rich layer with dPEP-rich droplets. The lateral growth of the pattern follows a $\lambda(t) = \lambda(t=0) + bt^{0.80}$ law where $\lambda(t=0)$ and $\lambda(t)$ are the pattern wavelength initially and at time $t$ after the quench.

## Introduction

Spinodal decomposition of polymer blends leading to patterned phase morphologies in the bulk is a fascinating subject that has been studied for the past two decades.[1−6] More recently, it has been realized that the presence of a surface breaks the rotational and translational symmetry, thus strongly altering both the equilibrium phase morphology and the phase separation kinetics.[7−9] Binary mixtures of polymers (for example, deuterated poly(ethylene propylene) (dPEP) and poly(ethylene propylene (hPEP)) are useful model systems to study these effects. For example, in a film of a two-phase isotopic polymer blend on a silicon substrate, preferential adsorption of the dPEP component to the surface and hPEP to the silicon leads to the formation of a macroscopic bilayer with the dPEP-rich phase wetting the surface and the hPEP-rich phase wetting the silicon.[10,11] In the early stages oscillatory composition profiles originate from both the surface and the substrate and propagate into the bulk of the film.[12−14] For compositions near the critical value, the wetting layer thickens as $a + bt^{1/3}$ where $t$ is the time after the quench, consistent with a process controlled by diffusive material exchange across the layer.[15,16] For off-critical quenches where the majority component wets the surface, the wetting layer grows faster, its thickness increasing approximately linearly with $t$. These kinetics are attributed to hydrodynamic transport by flow of dPEP through a perforated layer of hPEP-rich domains just below the dPEP-rich wetting layer.[17−19]

Experiments and simulations designed to probe the growth of lateral surface domains have uncovered quite different pieces of information. The lateral phase separation process within the film can be tracked by monitoring either surface height patterns,[20] elasticity differences of the phases,[21] or optical contrast.[22] Roughening of the air−polymer surface is even found in phase-separating films where the equilibrium film is smooth.[23,24] Numerical simulations allowing only diffusional transport reveal the same $t^{1/3}$ diffusion-limited growth usually found for bulk domains during spinodal decomposition.[16,25] Experiments on a critical mixture of deuterated polystyrene and partially brominated polystyrene seem to confirm this lateral growth behavior.[22]

Other experiments have shown an accelerated lateral growth of surface domains with exponents ranging from 1.1 to 1.5, depending on the quench depth.[26] Here fast and slow growth modes for phase separation under the influence of wetting coexist. Tanaka demonstrates that the slow growth mode could be induced by the bicontinuous phase separation itself.[27] Troian explains the larger exponents through constraints a wall imposes onto regular Lifshitz−Slyozov type coalescence.[28] Brown et al. observed a novel phenomenon in simulations on systems quenched into the metastable region where the majority phase is attracted by the surface. Domains of the minority phase may form much earlier in the near surface region than in the bulk.[29] A central assumption in Brown and Chakrabarti's theoretical treatment is that material exchange occurs solely by diffusion. In the present study we experimentally investigate this exact

10.1021/ma981709h CCC: $18.00 
Published on Web 05/14/1999

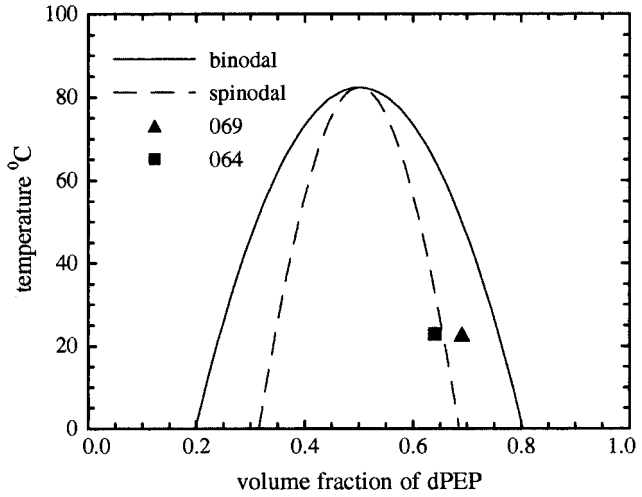


**Figure 1.** dPEP/hPEP phase diagram as determined experimentally for a film of around 4000 Å thickness. The quench locations of samples 064 and 069 are indicated. The spinodal line is determined from the $\chi$ determined from the binodal using the Flory−Huggins expression for the free energy.

case in an isotopic polymer blend and compare it to a quench into the unstable region. Laterally averaged depth profiles are measured by time-of-flight forward recoil spectrometry (TOF-FRES). The growth of the domains is accompanied by surface roughening. The topography of this surface roughness was characterized by scanning force microscopy (SFM).

## Experimental Procedure

The system under investigation is a mixture of poly(ethylene propylene) (PEP) and its deuterated analogue (dPEP). The degrees of polymerization are $N_{hPEP} = 2250$ and $N_{dPEP} = 2360$. These isotopic mixtures are characterized by a small positive interaction parameter $\chi$ due to differences in bond length and polarizability of the C−D bond and the C−H bond.[30] For the molecular weights used an upper critical solution temperature (UCST) of 365 K is found.[31] The difference in bond length and polarizability also causes the surface energy of the dPEP to be slightly less than that of the hPEP, thus providing a driving force for segregation of dPEP to the surface.[32,33]

Films approximately 1500 nm thick with dPEP volume fractions $\Phi_{dPEP} = 0.69$ and $\Phi_{dPEP} = 0.64$ were spun-cast from solution in toluene to silicon substrates. The thickness varies slightly from sample to sample due to experimental uncertainties in preparing films of this thickness. The dPEP/hPEP phase diagram (i.e., the binodal) has been determined experimentally for 400 nm thick films of this polymer mixture and is shown in Figure 1. An annealing temperature of 294 K was chosen. This corresponds to a quench depth of $0.81T_c$. The phase diagram shown in Figure 1 was determined by first finding the equilibrium binodal composition using 2D-time-of-flight forward recoil spectrometry (see below) and computing the spinodal composition from this binodal composition using the Flory−Huggins free energy of mixing; i.e., we use the binodal composition to determine the Flory parameter $\chi$.[34] As can be seen in Figure 1, the overall composition of one of the samples used for this study falls within the metastable region of the phase diagram, i.e., between spinodal and binodal. The overall composition of the other sample lies inside the unstable region of the phase diagram. The films were annealed in a vacuum for various times ranging from 1.5 h up to several weeks. The sample with dPEP volume fraction $\Phi_{dPEP} = 0.69$ is within the metastable region and in future is referred to as sample 069; the other sample is in the unstable region and is referred to as sample 064.

Composition versus depth profiles were established using 2D-time-of-flight forward recoil spectrometry (2D-TOF-FRES). In forward recoil spectrometry H and D nuclei recoil elastically

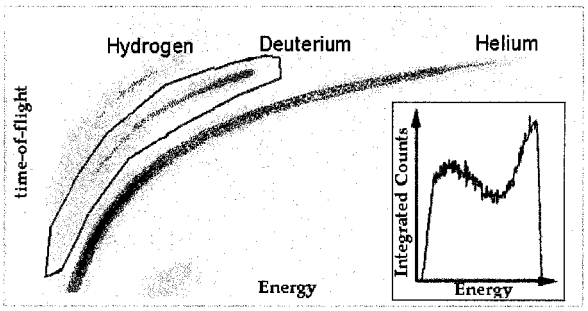


**Figure 2.** The 2-D-TOF−FRES spectrum. Counts are recorded versus energy and time-of-flight. The different elements fall inside different "mass bands". We can select a region in the 2-D spectrum and then integrate the counts over the time channels in the selected region and project the integrated counts onto the energy axis. We show the result of this procedure for the circled deuterium mass band in the inset.

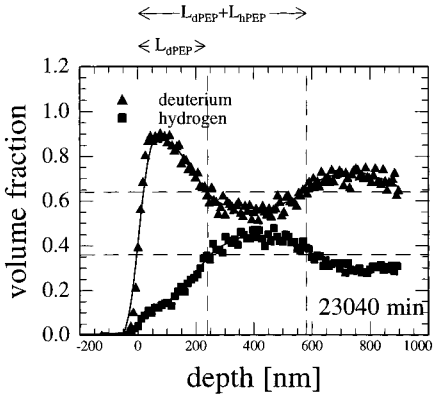


**Figure 3.** dPEP and hPEP volume fractions of sample 064 after 23 040 min of annealing as obtained from a 2-D-TOF-FRES spectrum. For best depth resolution in the near surface region the maximum depth we can probe is approximately 1000 nm. The solid curves are guides to the eye and are obtained by smoothing the data. From the intersections of the solid curve with the dashed horizontal lines indicating the initial dPEP and hPEP concentrations, we define a wetting layer and nucleation layer thickness $L_{dPEP}$ and $L_{hPEP}$.

in a forward direction from collisions with particles of an incident $He^{2+}$ beam. The energy of the outgoing particles is measured.[35,36] In 2D-TOF−FRES we also measure the flight time of the particles, and counts are recorded versus energy and time-of-flight.[37] The different masses of hydrogen, deuterium, and helium result in different energy versus time-of-flight dispersion relations, and the different particles can be easily identified in the spectrum (Figure 2). Due to the energy loss of particles penetrating into the sample, particles recoiled from the surface of the sample have a higher energy than particles recoiled from inside the sample. By projecting the counts for a certain particle onto the energy axis and converting energy loss into depth, a volume fraction versus depth profile can be obtained for each isotope (Figure 3). After the ion beam analysis of the sample, the topography of its surface was examined with scanning force microscopy (SFM) using a Nanoscope III SFM from Digital Instruments. The instrument was used in constant force mode. We used a $Si_3N_4$ cantilever tip with a nominal force constant of 0.06 N $m^{-1}$. The prior ion beam exposure cross-links the film, both "freezing" the phase morphology and allowing SFM of the now cross-linked elastomeric film to be performed without generating artifacts due to polymer flow.

## Results

Figure 4a shows TOF-FRES depth profiles for the 69% dPEP mixture for different annealing times. As dPEP segregates to the film−vacuum interface, a layer

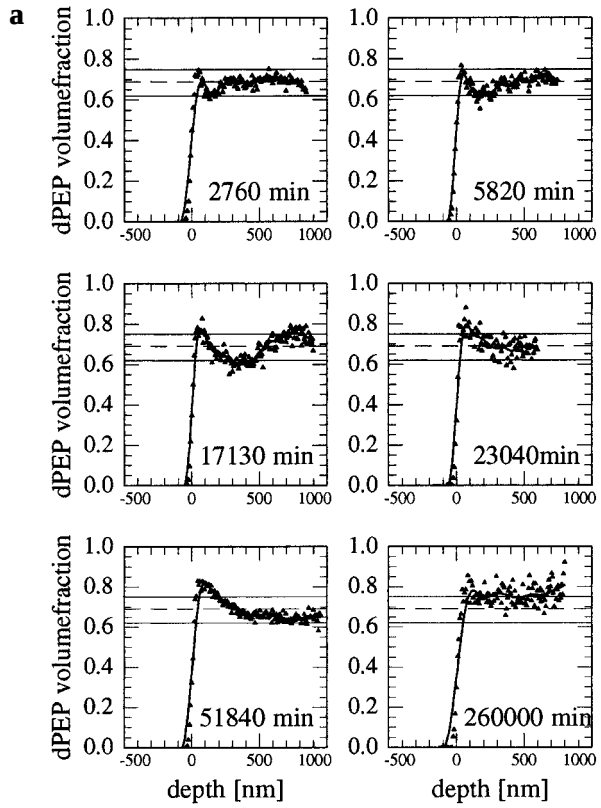
a
dPEP volumefraction
2760 min
5820 min
17130 min
23040min
51840 min
260000 min
depth [nm]
depth [nm]

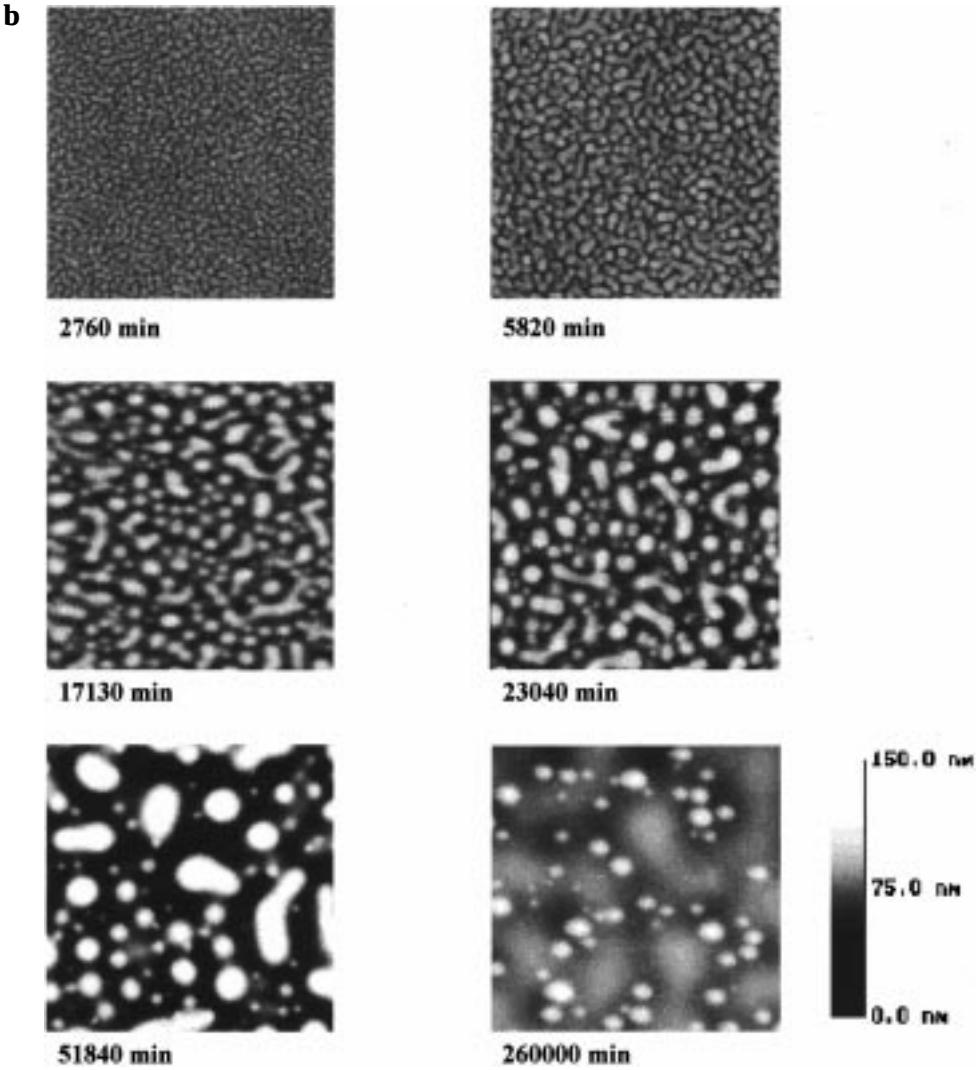
b
2760 min
5820 min
17130 min
23040 min
51840 min
260000 min
150.0 nm
75.0 nm
0.0 nm

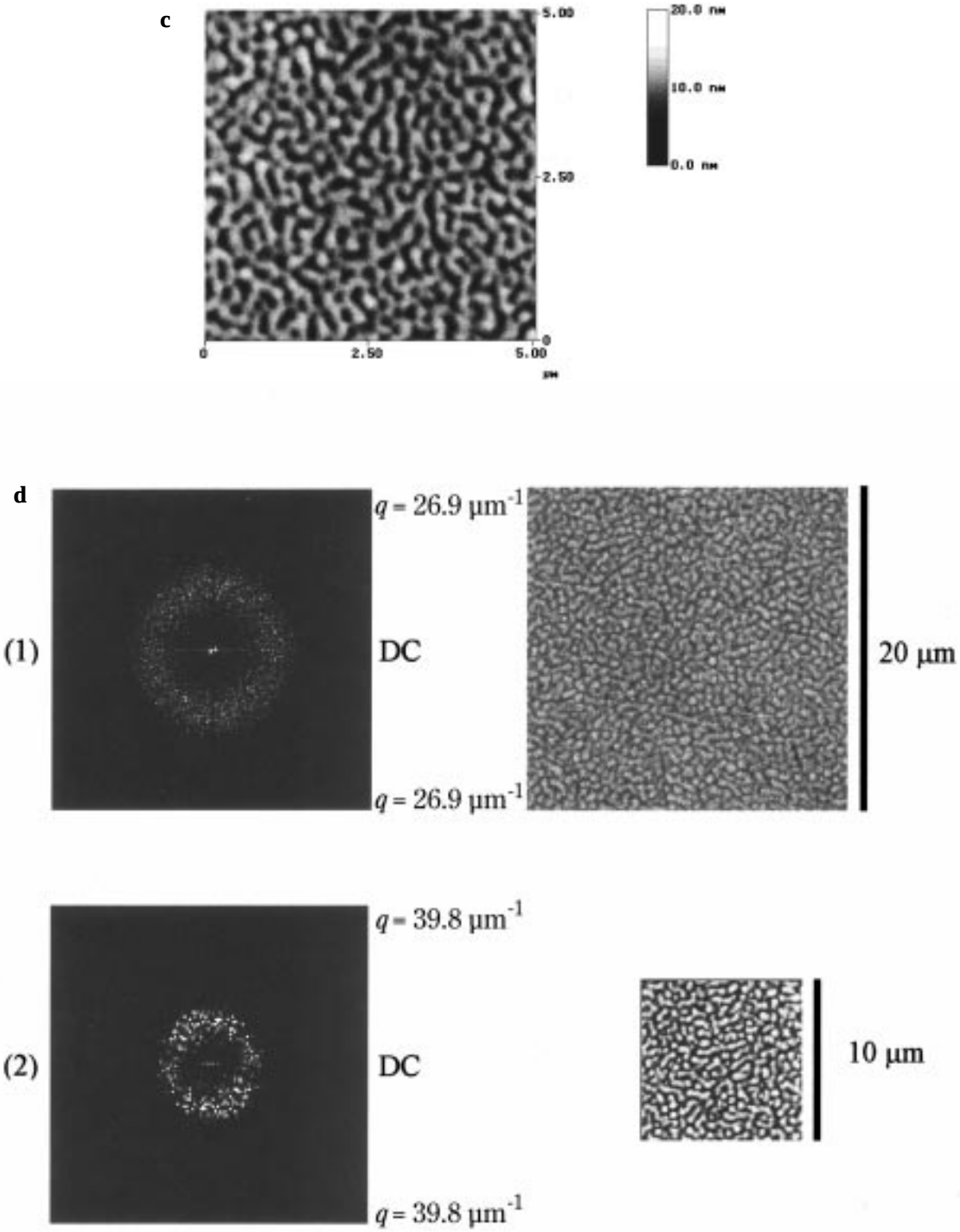


**Figure 4.** (a) Time evolution of the dPEP volume fractions for the sample 069 at 294 K. The dashed horizontal line indicates the initial volume fraction, while the solid horizontal lines indicate our estimate of the binodal and spinodal compositions for this film thickness. (b) Time evolution of the surface morphologies for the samples shown in (a). The base side of the SFM scans is 20 $\mu$m. For all SFM scans the surface features lie within the $z$-range of 150 nm. (c) Bicontinuous surface pattern as formed after 360 min of annealing. The base side of the SFM scan is 5 $\mu$m. (d) Power spectra of the phase pattern after 2760 min for images of different sizes: (1) and (2) have a base length of 20 and 10 $\mu$m, respectively.

depleted in the dPEP component forms next to the wetting layer (Figure 4a, $t$ = 2760 min). After further annealing the wetting and the depletion layers thicken, and the concentration in the depletion layer falls below the spinodal concentration (Figure 4a, $t$ = 5820 min). In the narrow depletion layer the composition of the film is in the unstable region of the phase diagram, while the interior of the film is still in the metastable region. In the interior of the sample nucleation and droplet growth due to interdiffusion may occur, but these processes are very slow compared to spinodal decomposition which occurs in the subsurface depletion layer.

Uphill diffusion from the unstable depletion layer actually increases the dPEP content of the layer below it, shifting the composition of this layer further from the spinodal. We thus find a three-layer structure inside the film: a dPEP-rich wetting layer, the unstable subsurface layer, and a dPEP-rich bulk region (Figure 4a, $t = 17\,130$ min). Upon further annealing this layer structure decays, and we observe a constant bulk volume fraction (which is still in the metastable region) and a surface segregation peak (Figure 4a, $t = 23\,040$ and $t = 51\,840$ min). In final equilibrium (Figure 4a, $t = 260\,000$ min) we find a macroscopic dPEP-rich layer against the vacuum interface. The dPEP volume fraction at this layer represents the binodal composition. Similarly, the hPEP-rich phase forms a macroscopic layer next to the substrate.

We now concern ourselves with the lateral phase separation in the subsurface depletion layer. Unfortunately, the similarity of the two components does not allow us to directly monitor the lateral composition of the film. In earlier experiments however we demonstrated that mass flow inside the phase separating film can result in height modulations of the surface that can be revealed with scanning force microscopy (SFM).[24] Figure 4b shows SFM scans corresponding to the depth profiles shown in Figure 4a. At the earlier times a bicontinuous structure typical of spinodal demixing can be seen. At later times the morphology transforms from an interconnected phase pattern to a droplet phase pattern, and we observe droplet coalescence. The height of the droplets increases with annealing time for the first 51 840 min. The roughness is significantly smaller at 260 000, min but the film surface is still not smooth, as would be expected for complete equilibrium.

The mechanism for surface pattern formation must somehow involve hydrodynamic flow, since this patterning is not observed for thick films of the critical composition for which the subsurface layer is a homogeneous hPEP-rich phase, through which diffusion controls the growth of the dPEP-rich wetting layer. We suggest the following 3D scenario: as soon as the subsurface layer falls into the unstable region of the phase diagram, a spinodal decomposition process starts within this layer. The domains forming are elongated (their cross section assumes an elliptical shape) as the domain growth takes place in a two-dimensional geometry confined between the wetting surface layer and the film interior. Driven by interfacial tension between the two phases, the cross section of these domains relaxes into a more circular shape as shown in Figure 5. This shape change exerts a pressure on the free (vacuum) surface of the film, and we observe undulations of the polymer−vacuum interface. Given this mechanism, an elevated surface indicates a minority phase droplet in the subsurface layer. Following the time evolution of the surface roughening, we can now understand why the depletion region decays: The closer the domains come to their equilibrium composition, the more the influence of the initial composition shows. As we are dealing with a composition far off the critical value, the initial bicontinuous 2D phase morphology evolves into a morphology of hPEP-rich minority phase droplets within the dPEP-rich majority phase (Figure 4b). As the wetting layer grows, the minority phase droplets slowly diffuse away from the surface to form a wetting layer at the substrate. We would like to highlight the reason why we believe that the lateral phase separation in the subsurface depletion layer is by spinodal decomposition rather than by nucleation and growth. The surface features we observe in the very early stages are bicontinuous, a morphology inconsistent with a nucleation and growth mechanism but exactly the morphology expected for a spinodal decomposition process (Figure 4c). In Figure 4d we give evidence that our phase separation is indeed a quasi-two-dimensional process.

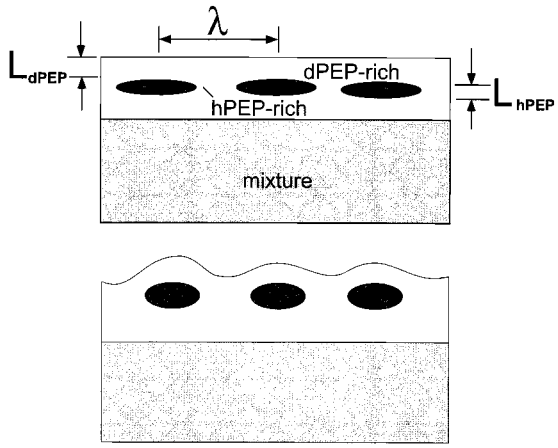


**Figure 5.** Schematic sketch illustrating the mechanism for surface roughening on isolated minority phase droplets. (a) The droplets have an elongated shape as the coarsening parallel to the surface accelerates. (b) Resulting equilibrium structure. The sketch also illustrates the main growth parameters.

As reported by Tanaka and Sigehuzi, confined phase-separating fluid mixtures have local orientational order.[38] For a large image (20 $\mu$m × 20 $\mu$m) the two-dimensional power spectrum $\vec{q}$ is isotropic, while $\vec{q}$ from a smaller region of the same image shows an anisotropic scattering pattern indicating the existence of local orientation (Figure 4d).

Figure 6a shows a time series of depth profiles for an initial composition of $\Phi_{dPEP} = 0.64$, a composition that is inside the unstable region of the phase diagram. The dPEP profiles show oscillations caused by surface-induced spinodal decomposition. After 23 040 min of annealing a surface wetting layer with a dPEP volume fraction of $\Phi_{dPEP} = 0.90$ is observed, followed by a depletion layer below it with a dPEP volume fraction of $\Phi_{dPEP} = 0.55$. The $\Phi_{dPEP}$ increases to 0.65 as we reach the interior of the film (Figure 6a, $t = 23\,040$ min). Finally, the film collapses into a bilayer with a dPEP-rich phase wetting the vacuum interface and a hPEP-rich phase wetting the substrate (Figure 6b, $t = 260\,000$ min). The existence of local orientation as observed in sample 069 is even more evident from the power spectrum $S(\vec{q})$ as plotted in the insets in Figure 6b. The spatial correlation is increased, as the composition is more symmetric.

Our results can be made more quantitative by observing the characteristic lengths as defined in Figures 3 and 5. The thickness of the wetting layer $L_{dPEP}(t)$ and the thickness of the unstable region $L_{hPEP}(t)$ are found from the TOF-FRES depth profiles (see Figure 3). The fact that minority phase domains only form in a narrow layer leads to a layering of hPEP-rich domains parallel to the substrate. As a consequence, coalescence and flow are favored in the plane parallel to the substrate, and the domains assume an elongated shape. A characteristic length $\lambda$ of the lateral surface pattern can be found from the AFM images by determining the peak position in the power spectral density.

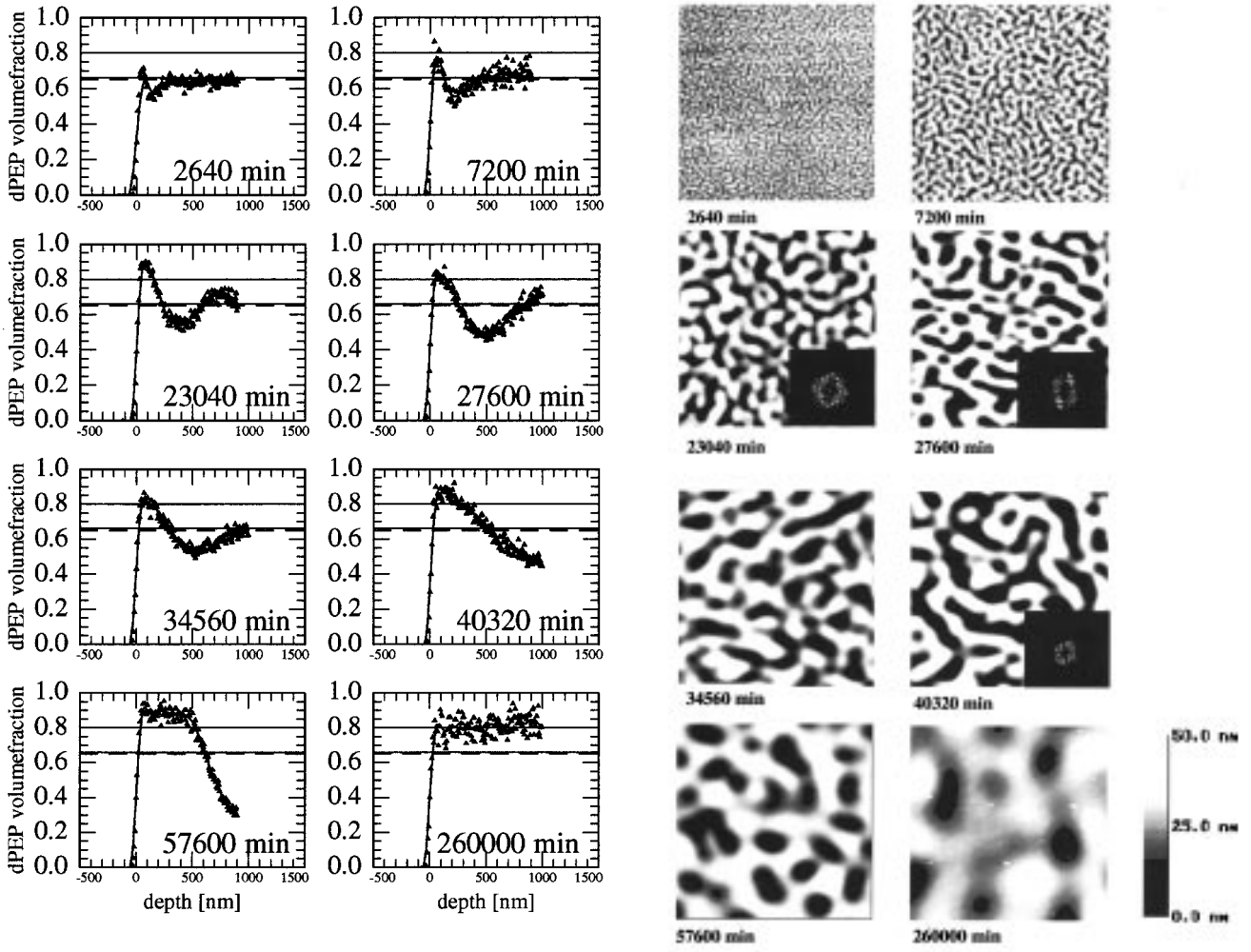


**Figure 6.** Time evolution of the dPEP volume fraction (a, left) and the surface morphologies (b, right) of the sample 064 at 294 K. The dashed horizontal line indicates the initial volume fraction, while the solid horizontal line indicates our estimate of the spinodal composition. The base side of the AFM scans is 20 $\mu$m. For all SFM scans the surface features lie within the *z*-range of 50 nm. In the insets of the real space images shown for 23 040, 27 600, and 40 300 min of annealing we show the corresponding FFT power spectra. The scale ranges from $q = -37.8$ to 37.8 $\mu m^{-1}$.

In Figure 7 we plot the time evolution for different characteristic lengths for both of the samples. It is seen that the relevant lengths behave the same in both of the samples. Over the whole time range the growth of the parameters is well represented by $l(t) = a + bt^n$. We perform a standard linear regression analysis on linearized scales (log−log presentation), where we select the individual error bars as weight (1/error squared). This procedure results in the following exponents: $n = 1.11 \pm 0.05$ ($n = 1.00 \pm 0.03$) for wetting layer growth and $n = 0.80 \pm 0.05$ ($n = 0.80 \pm 0.03$) for surface pattern evolution for sample 064 (069), respectively. The errors are the standard deviation of the best linear fit. $\lambda$ is almost 1 order of magnitude larger than the characteristic length of the composition modulation perpendicular to the sample surface.

## Discussion

While previous studies of the phase separation of isotopic polymer blends in thin films have revealed a detailed picture of the morphology and kinetics normal to the film, information about the lateral phase structure of isotopic systems has not been readily available. Methods that reveal contrast between hydrogen and deuterium or between C−H and C−D bonds (e.g., Raman spectroscopy) do not have sufficient lateral resolution to image the lateral structure. However, our experiments reported above show that for off-critical dPEP/hPEP blends the phase separation process is accompanied by transient surface roughening which can easily be investigated with scanning force microscopy.[24] Careful comparison of the depth profiles and the surface structure allows us to infer information about the lateral phase structure in the near surface region. The roughening is only observed for off-critical (dPEP-rich) mixtures where the major component wets the surface. Thick films of symmetric mixtures of dPEP/hPEP or mixtures whose minority component wets the surface do not show surface roughening.

One of the characteristics of spinodal decomposition is the existence of a dominant time-dependent heterogeneity length $L_m = 2\pi/q_m$ that describes the composition fluctuations.[39] At $t = 0$ this can be calculated using an extension of the Cahn−Cook linearized theory of spinodal decomposition[40] to polymer blends:[1−3]

$$q_m^2(t=0) = \frac{3}{2R_g^2}\left(\frac{\chi}{\chi_s} - 1\right) \qquad (1)$$

Kedrowski et al. report measurements on the same polymer blend at the critical composition.[41] Small-angle neutron scattering (SANS) measurements on this PEP

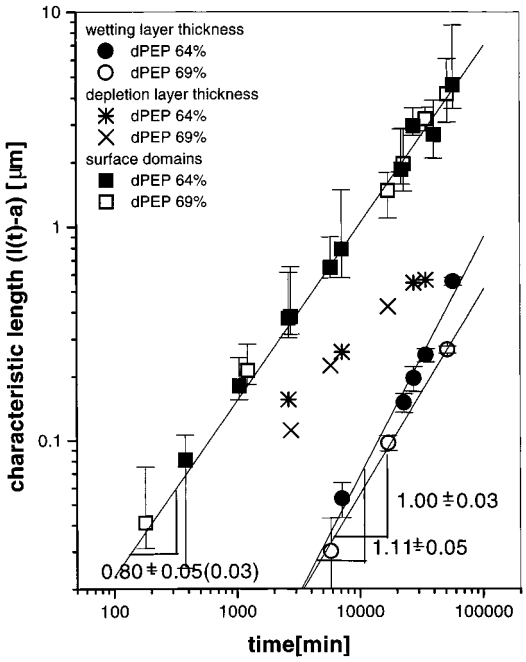


**Figure 7.** Wetting layer thickness $L_{dPEP}$, the thickness of the subsurface depletion layer $L_{hPEP}$, and lateral dimensions $\lambda$ of the hPEP-rich domains in samples 064 and 069. We assume a shape of $l(t) = a + bt^n$. To obtain the exponents, we plot log-($l(t) - a$) over log($t$). Results are obtained by TOF-FRES for $L_{dPEP}$ and SFM for $\lambda$.

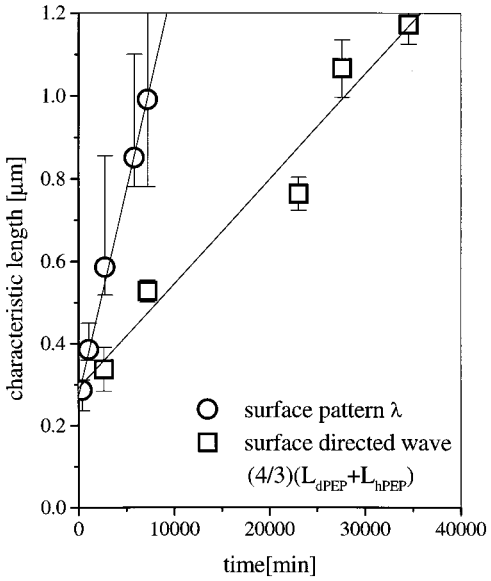


**Figure 8.** Early stages of the development of spinodal pattern for sample 064. We show the wavelength of the spinodal wave $^4/_3(L_{dPEP} + L_{hPEP})$ and the characteristic length of the surface pattern $\lambda$.

mixture[31] yielded

$$\chi = a/T + b = 0.568/T - 6.62 \times 10^{-4} \qquad (2)$$

for the Flory−Huggins interaction parameter and $R_g$ = 155 Å for the radius of gyration. We calculate the value of the interaction parameter on the spinodal by

$$\chi_s = \frac{2}{N\Phi} + \frac{2}{N(1-\Phi)} \qquad (3)$$

With $N = 2250$ we find $L_m(t{=}0) = 1400$ Å for $\Phi = 0.64$ and $L_m(t{=}0) = 1730$ Å for $\Phi = 0.69$ for bulk dPEP/PEP mixtures. Our thin-film experiments have produced two different length scales, which we can compare to the theoretical evaluations: a lateral characteristic length $\lambda$ and a spinodal wavelength $^4/_3(L_{dPEP} + L_{hPEP})$ perpendicular to the surface. The comparison can only be qualitative because our experiments cannot directly access the initial linear regime at short times and because the thermodynamics of the blend are altered by the thin-film nature of the sample.[36] The $t = 0$ intercept of the linear fits of $\lambda(t)$ and $^4/_3(L_{dPEP} + L_{hPEP})$-($t$) in the early stages (Figure 8) yields initial characteristic lengths of $\lambda(t{=}0) = 2740$ Å and $^4/_3(L_{dPEP} + L_{hPEP})(t{=}0) = 2920$ Å. The rough agreement with the theory lends further support to the assumption that we observe spinodal fluctuations perpendicular as well as parallel to the surface. Despite the fact that the initial wavelengths of the normal and lateral structures are similar, the wavelength grows much faster in time parallel to the substrate.

The wetting layer forms by hydrodynamic flow of dPEP through dPEP-rich bicontinuous tubes, and at the same time the bicontinuous pattern in the subsurface layer coarsens with time. Potential driving forces for the growth of the wetting layer are either the Laplace pressure in the interior of the film[42] or a repulsive van der Waals force across a dPEP-rich surface layer.[43] An analysis of a similar problem using the capillary pressure as a driving force has been given by Guenon et al.[42] As there is a viscous resistance to the flow, we should solve for the $x$-component of the Navier−Stokes equation for both approaches,

$$\nabla p_x = \eta \Delta v_x \qquad (4)$$

For a more detailed analysis we need to make assumptions about the exact geometry and time evolution of the width of the perforations through which the flow occurs. Unfortunately, this information is experimentally not accessible, and the validity of this type of analysis remains questionable, even though we can find agreement with the experiments.

Another issue of interest is why the scale of the lateral surface pattern coarsens much faster than the composition wave normal to the surface (see Figure 8). A possible explanation is that the mean composition $\langle\Phi\rangle$ about which the wave normal to the surface develops is close to the spinodal so that the quench depth is small, where the quench depth is $(T_s(\langle\Phi\rangle) - T)/T_s(\langle\Phi\rangle)$, where $T_s(\langle\Phi\rangle)$ and $T$ are the spinodal temperature at $\langle\Phi\rangle$ and the actual temperature, respectively. This small quench depth should produce relatively slow kinetics of coarsening. On the other hand, the average local composition $\langle\Phi_{sub}\rangle$ in the hPEP-rich subsurface layer is far inside the spinodal so that the quench depth $(T_s(\langle\Phi_{sub}\rangle) - T)/T_s(\langle\Phi_{sub}\rangle)$ within this layer is larger. This larger quench depth should produce relatively rapid coarsening of the two-dimensional spinodal decomposition morphology within the subsurface hPEP-rich layer.

In summary, we have investigated the near surface phase separation of an off-critical polymer mixture where lateral spinodal decomposition was induced in the very narrow depletion layer adjacent to a surface wetting layer. Spinodal patterns develop, but their growth is confined to this depletion layer. We investigated two different initial compositions. If we start with a film of metastable composition, the depletion region quickly decays, and the lateral pattern, which was

initially bicontinuous, transforms into minority phase droplets. On the other hand, if we start with an initial composition inside the unstable region, surface directed spinodal decomposition drives the composition of the depletion layer further away from the dPEP-rich phase composition. Accordingly, the bicontinuous pattern transforms into a hPEP-rich layer. The wetting layer thickness and the wavelength of the lateral pattern follow nearly the same growth law. This can be accounted for by solving the Navier−Stokes equation if both the wetting layer thickness and the lateral pattern grow by hydrodynamic flow processes.

**Acknowledgment.** We gratefully acknowledge primary funding for this work from the National Science Foundation Polymers Program NSF-DMR Grant 9803738 (E.J.K., J.H.) and 9405101 (F.S.B.). We also acknowledge the use of the Ion Beam Facility and the scanning force microscope of the Cornell Center for Materials Research which is funded by NSF-DMR-9632275 and NRC COBASE program. The skillful help of Nick Szabo during the TOF-FRES experiments is gratefully acknowledged. The authors also thank Glenn Fredrickson and Gary Leal for illuminating discussions.

## References and Notes

(1) de Gennes, P. G. *J. Chem. Phys.* **1980**, *72*, 4756.
(2) Pincus, P. *J. Chem. Phys.* **1981**, *75*, 1996.
(3) Binder, K. *J. Chem. Phys.* **1983,** *79*, 6387.
(4) de Gennes, P. G. *Rev. Mod. Phys.* **1985**, *57*, 827.
(5) Bates, F. S.; Wiltzius, P.; Heffner, W. R. *Phys. Rev. Lett.* **1988**, *60*, 1538.
(6) Wiltzius, P.; Bates, F. S. *J. Chem. Phys.* **1989**, *91*, 3258.
(7) Klein, J. *Science* **1990**, *250*, 640.
(8) Steiner, U.; Eiser, E.; Klein, J.; Budkowski, A.; Fetters, L. J. *Science* **1992,** *258*, 1126.
(9) Krausch, G. *Mater. Sci. Eng. Rep.* **1995,** *R14*, 1.
(10) Schmidt, I.; Binder, K. *J. Phys. (Paris)* **1985**, *46*, 1631.
(11) Krausch, G.; Dai, C.-A.; Kramer E. J.; Marko, J. F.; Bates, F. S. *Macromolecules* **1993,** *26*, 5566.
(12) Ball, R. C.; Essery, R. L. H. *J. Phys.: Condens. Matter* **1990**, *2*, 10303.
(13) Jones, R. A. L.; Norton, L. J.; Kramer, E. J.; Bates, F. S.; Wiltzius, P. *Phys. Rev. Lett.* **1991,** *66*, 1326.
(14) Puri, S.; Binder, K. *Phys. Rev. A* **1992**, *46*, R4487.
(15) Krausch, G.; Dai, C.-A.; Kramer, E. J.; Bates, F. S. *Phys. Rev. Lett.* **1993,** *71*, 3669.
(16) Brown, G.; Chakrabarti, A. *Phys. Rev. A* **1992**, *46*, 4829.
(17) Krausch, G.; Kramer, E. J.; Bates, F. S.; Marko, J. F.; Brown, G.; Chakrabarti, A. *Macromolecules* **1994,** *27*, 6768.
(18) Marko, J. F. *Phys. Rev. E* **1993**, *48*, 2861.
(19) Siggia, E. D. *Phys. Rev. A* **1979**, *20*, 595.
(20) Karim, A.; Slawecki, T. M.; Kumar, S. K.; Douglas, J. F.; Satija, S. K.; Han, C. C.; Russell, T. P.; Liu, Y.; Overney, R.; Sokolov, J.; Rafailovich, M. H. *Macromolecules* **1998,** *31*, 857.
(21) Marti, O.; Colchero, J.; Mlynek, J. *Nanotechnology* **1990**, *1*, 141. Krausch, G.; Hipp, M.; Boeltau, M.; Marti, O.; Mlynek, J. *Macromolecules* **1995,** *28*, 260.
(22) Bruder, F.; Brenn, R. *Phys. Rev. Lett.* **1992,** *69*, 624.
(23) Steiner, U.; Klein, J.; Fetters, L. J. *Phys. Rev. Lett.* **1994**, *72*, 1498.
(24) Jandt, K. D.; Heier, J.; Bates, F. S.; Kramer, E. J. *Langmuir* **1996**, *12*, 3716.
(25) Toral, R.; Chakrabarti, A. *Phys. Rev. B* **1991,** *43*, 3438.
(26) Cumming, A.; Wiltzius, P.; Bates, F. S.; Rosedale, J. H. *Phys. Rev. A* **1992,** *45*, 885. Wiltzius, P.; Cumming, A. *Phys. Rev. Lett.* **1991,** *66*, 3000.
(27) Tanaka, H. *Phys. Rev. Lett.* **1994**, *72*, 3690.
(28) Troian, S. M. *Phys. Rev. Lett.* **1993**, *71*, 1399.
(29) Brown, G.; Chakrabarti, A.; Marko, J. F. *Phys. Rev. E* **1994**, *50*, 1674.
(30) Bates, F. S.; Wignall, G. D.; Koehler, W. C. *Phys. Rev. Lett.* **1985,** *55*, 2425.
(31) Gehlsen, M. D.; Rosedale, J. H.; Bates, F. S.; Wignall, G. D.; Hansen, L.; Almdahl, J. *Phys. Rev. Lett.* **1992,** *68*, 2452.
(32) Bartell, L. S.; Roskos, R. R. *J. Chem. Phys.* **1966,** *44*.
(33) Jones, R. A. L.; Norton, L. J.; Kramer, E. J.; Composto, R. J.; Stein, R. S.; Russell, T. P.; Mansour, A.; Karim, A.; Felcher, G. P.; Rafailovich, M. H.; Sokolov, J.; Zhao, X.; Schwarz, S. A. *Europhys. Lett.* **1990,** *12*, 41.
(34) Heier, J.; Genzer, J.; Kramer, E. J.; Krausch, G., unpublished results. The equilibrium binodal compositions measured in this study fall well inside the coexistence curve as predicted by mean field theory from the measured $\chi$ parameter. We have evidence that the finite film thickness alters the binodal values.
(35) Doyle, B. L.; Peercy, P. S. *Appl. Phys. Lett.* **1979**, *34*, 811.
(36) Mills, P. J.; Green, P. F.; Palmstrom, C. J.; Mayer, J. W.; Kramer, E. J. *Appl. Phys. Lett.* **1984,** *45*, 957.
(37) Sokolov, J.; Rafailovich, M. H.; Jones, R. A. L.; Kramer, E. J. *Appl. Phys. Lett.* **1989**, *54*, 590.
(38) Tanaka, H.; Sigehuzi, T. *Phys. Rev. E* **1995**, *52*, 829.
(39) Cahn, J. W. *J. Chem. Phys.* **1965**, *42*, 93. Cahn, J. W. *Trans. Metall. Soc. AIME* **1968,** *242*, 166.
(40) Cook, H. E. *Acta Metall.* **1970**, *18*, 297.
(41) Kedrowski, C.; Bates, F. S.; Wiltzius, P. *Macromolecules* **1993**, *26*, 3448.
(42) Guenoun, P.; Beysens, D.; Robert, M. *Phys. Rev. Lett.* **1990**, *65*, 2406.
(43) Israelachvili, J. *Intermolecular & Surface Forces*, 2nd ed.; Academic Press: London, 1992.

MA981709H